



Texture and Tensile Properties of Three-Layered Titanium Clad–AZ31 Magnesium Alloy Sheet by Single-Pass Hot Rolling

Baleegh Alobaid¹

Received: 14 December 2022 / Revised: 3 March 2023 / Accepted: 8 March 2023 / Published online: 23 March 2023
© ASM International 2023

Abstract

In the present study, a three-layered Ti/AZ31/Ti clad sheet was produced by single-pass hot rolling. Metallurgical bonding between Ti and AZ31 was successfully achieved with a reduction of thickness 38% (sheet I) and 50% (sheet II). The microstructure and mechanical behavior were analyzed using optical microscopy (OM), X-ray diffraction (XRD), scanning electron microscopy (SEM), energy dispersive spectroscopy (EDS), electron backscatter diffraction (EBSD), nanoindentation, and tensile tests. The AZ31 layer in sheets I and II exhibited microstructures of shear bands and tensile twins $\{10\bar{1}2\}\langle 10\bar{1}1\rangle$. The shear bands acted as local strain concentration areas which led to the failure of the clad sheets with limited elongation. Heat treatment caused changes in the microstructure and mechanical properties of clad sheets due to static recrystallization (SRX) on twins and shear bands in the AZ31 layer. Recrystallized grains usually randomize the texture which led to weaken the strong deformed (0001) basal texture. Twins served as nucleation sites for grain growth during SRX. Tensile tests at room temperature showed significantly improved ductility of the clad sheets after heat treatment at 400 °C for 12 h. The results showed that the mechanical properties of clad sheet II are better than clad sheet I: Clad sheet II shows elongation 13% and 35% along the rolling direction (RD) for as-rolled and annealed clad sheet, respectively, whereas clad sheet I shows elongation 10% and 22% along RD for as-rolled and annealed clad sheet, respectively.

Keywords Three-layered Ti/AZ31/Ti · Clad sheet · Heat Treatment · Static recrystallization (SRX) · Mechanical Behavior

Introduction

Severe plastic deformation (SPD) is an effective method for achieving high strength and high ductility of Mg alloys with very fine grain sizes. However, the application of Mg alloys is quite limited because of poor corrosion resistance. Magnesium composite materials have been produced with various materials such as Al [1], Zn [2, 3], Ni [4], and Cu [5] to improve their mechanical and heat conductivity properties. Also, Mg alloys have been clad by various types of materials such as aluminum [6, 7], steel [8], and titanium [9–11]. Metal–metal composite materials were fabricated by bonding multilayers, which have the advantage of their mechanical properties. Kawamoto et al. [12] studied strain transfer through the Mg/Ti interface using a crystallographic

method. They suggested that the dispersion of Ti particles in the Mg-based composite can improve the deformability of Mg by the strain transfer through the Mg/Ti interface [13]. Clad sheets component is minimized Mg alloys weakness and provides a new application area. The ductile layer can attribute to prevent failure of a less ductile layer of metal–metal composite materials, which will be necking at the higher strain that depends on the two metals [8]. Therefore, it is important to obtain a suitable method to fabricate Ti/AZ31/Ti Clad sheet. There are many processes to manufacture Mg multilayer composite materials such as accumulative roll bonding (ARB) [1, 14], diffusion bonding (DB) [15, 16], brazing and friction stir welding [17–23], and roll bonding (RB) [7, 24]. The roll bonding process has been reported as a conventional method to fabricate and bond clad sheet by cold or warm rolling [25]. The strength of bi-metal composites depends on the volume fraction of its constituent. This is mainly associated with bonding strength between different constituents, which can increase the strength of the material [26].

✉ Baleegh Alobaid
baleegh.saud@mu.edu.iq

¹ College of Engineering, Al-Muthanna University, Samawah, Muthanna 66001, Iraq

In the present work, the Ti/AZ31/Ti clad sheet was fabricated by single-pass hot rolling. AZ31 Mg alloy has relatively poor tensile ductility; therefore, utilizing the advantages of both Mg and Ti may improve its performance in structural applications. Moreover, clad sheet gains the corrosion resistance equivalent to that of Ti alloys. The microstructure and mechanical properties of the clad sheet Ti/AZ31/Ti were investigated. Mainly, the Ti/AZ31 interface texture orientation was studied as well. The relation between texture and mechanical properties at the interface was discussed.

Experimental Procedures

The materials were used commercially pure Ti grade 2 (Ulbricht) (C 0.012, N 0.005, Fe 0.09 and balance Ti wt.%) and AZ31B magnesium alloy (Magnesium Electron) (Al 3.06, Zn 1.04, Mn 0.4, Cu 0.001, Si 0.004, Fe 0.0035, and balance Mg wt.%). Three layered, Ti/AZ31/Ti clad sheet, was produced by single-pass hot rolling. The AZ31 and Ti sheets were cut into rectangular pieces of $75 \times 50 \times 3.06 \pm 0.10$ mm and $75 \times 50 \times 0.2 \pm 0.02$ mm, respectively. Sandwiched samples were heated in a furnace at 450°C for 15 min and then fed through a rolling mill with a reduction of thickness 38% and 50% in a single pass, as shown in Fig. 1a. The samples named as the clad sheet I and II for reduction of thickness 38% and 50%, respectively. The AZ31 and Ti plates were degreased by an ultrasound bath using acetone for 15 min and roughed by using a rotating stainless steel wire brush before assembly. Samples surface preparations were carried out to achieve a good bonding strength between layers. The degreasing and surface roughing steps were required to avoid sheets

sliding to obtain an excellent bonding strength between layers [27]. The roller diameter was 101.6 mm, and the rotational speed of the roller was 24 revolutions per minute. Heat treatment was carried out in an argon atmosphere furnace at 400°C for 12 h.

The Ti clad Mg alloy sheets were observed along the (TD) plane using optical microscopy (OM), scanning electron microscopy (SEM), X-ray diffraction (XRD), energy dispersive X-ray (EDX), and electron backscattering diffraction (EBSD) patterns. Samples were ground using silicon carbide abrasive papers of grit sizes 320, 1200 and 2000. Preparations of EBSD samples were difficult because the Ti and AZ31 required different solutions and methods for surface polishing. Therefore, the polishing was performed layer by layer. Suter's electrochemical polisher was employed to polish the AZ31 layer; an electrolyte (methanol: ethanol: nitric acid = 10:10:3) at room temperature and voltage of 27–30 V. Ti layers were chemically polished using (nitric acid: hydrofluoric acid = 1:1) to obtain high-quality EBSD patterns [28, 29]. EBSD was performed on the as-rolled and annealed samples using FEI (Helios NanoLab 660) equipped with an electron backscatter diffraction (EBSD) system. The EBSD data were analyzed using HKL channel 5 software. The mechanical behavior was evaluated by nanoindentation (Agilent G200) and tensile test. The tensile test samples were cut parallel to both (RD) and (TD) directions. The tensile strength test was performed at room temperature using (Instron 3345 machine) machine with an initial strain rate of 0.5 mm/min. The tensile test spacemen were machined by an electric discharge machine (EDM) and have a gauge length of 10 mm and 2 mm width, as shown in Fig. 1b [30].

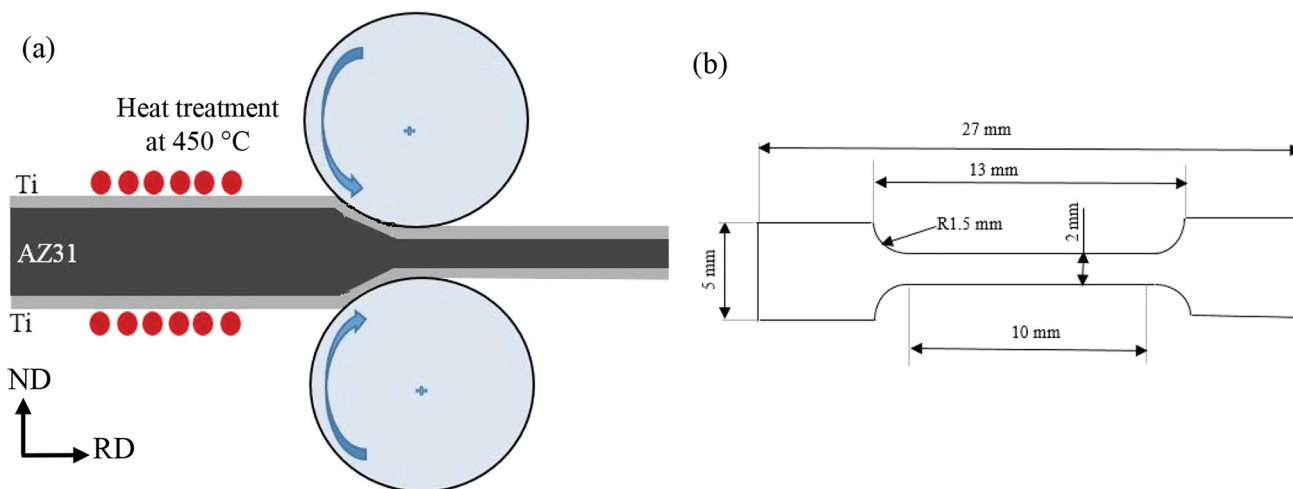


Fig. 1 (a) illustration of the fabrication of Ti/AZ31 clad sheet; (b) dimensions of the tensile test specimens

Results and Discussion

Microstructural Characterization

Ti/AZ31/Ti clad sheets were fabricated with a thickness reduction of 38% and 50% (sheet I and II). Optical microscopy (OM) observations appear without any visible defects such as pores, voids, cracks, interface debonding, or delamination, as shown in Fig. 2a. Considering high plastic deformation generated at the interface which causes a zig-zag mode at the interface due to different flow stress of the Ti and AZ31. The interfacial zig-zag mode is a favor geometrical shape that enhances the bonding strength between layers [25, 27, 31].

It is suggested that plastic deformation and friction could increase the temperature at the interface. This lead to softening of both the Ti and the AZ31 and increases the plastic strain as well as the migration of atoms across the AZ31/Ti interfaces [4, 24]. Figure 2b shows microstructure of the as-rolled clad sheet which is observed as a mixed microstructure of parallel shear bands inclined by $\pm 35^\circ$ and tensile twins $\{10\bar{1}2\}\langle 10\bar{1}1\rangle$ in areas far from the interface of

the Ti/AZ31 layer. While ultrafine dynamic recrystallization (DRX) grains were found close to the Ti/AZ31 interface, a high friction interaction between both layers occurs during the rolling; that means the main deformation mechanisms during hot rolling where controlled by basal $\langle a \rangle$ slip system ($\{0001\}\langle 11\bar{2}0 \rangle$) and twinning $\{11\bar{2}0\}$ [32, 33]. Figure 2c illustrates microstructure of the as-rolled AZ31 sheet with reduction of thickness 50%. DRX occurred during the hot rolling which produced homogenous equiaxed fine grains with small fractions of shear bands, as previously reported [34–38]. Compared with the as-rolled clad sheet microstructure, the clad sheet samples were deformed under the high strain rate along the normal direction (ND) which was generated the shear bands (many fine DRX grains) and twins microstructures [39]. The shear bands act as local strain concentration areas which lead to fail the clad sheet with lower elongation [40–42]. Annealing of the clad sheets can improve the ductility of the Z31 layer and the bonding strength between the Ti and AZ31 [9]. Further annealing, the microstructures of the AZ31 layer showed uniform equiaxed recrystallized grains, as shown in Fig. 2d. Optical microscopy cannot provide high magnification views of shear bands. SEM of shear bands is shown in Fig. 3. The

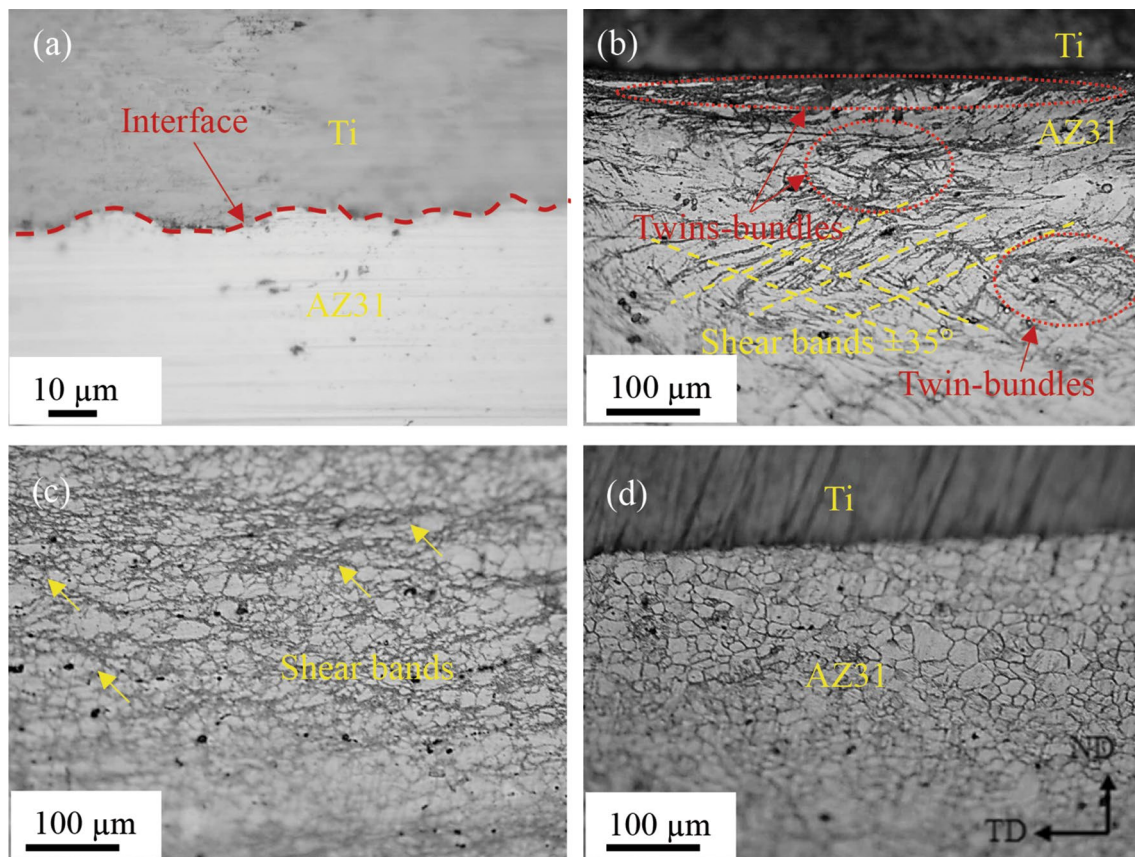


Fig. 2 OM images of the Ti/AZ31 interfaces; (a, b) as-rolled clad sheet II; (c) AZ31 hot rolled with 50% reduction; (d) annealed clad sheet II

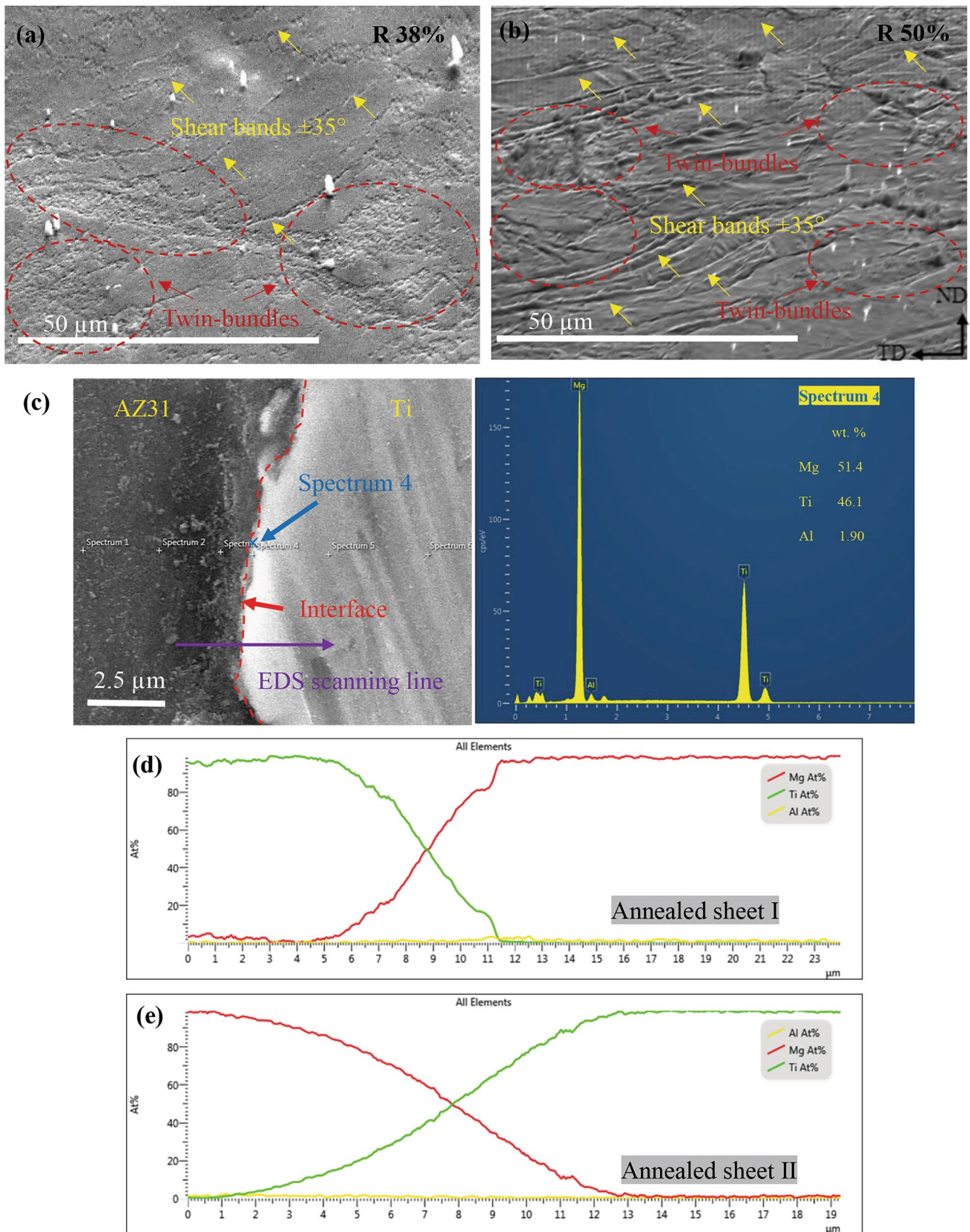


Fig. 3 Shows SEM images: **(a)** sheet I as-rolled AZ31 layer; **(b)** sheet II as-rolled AZ31; **(c)** point scanning of annealed sheet II interface; **(d, e)** line scanning of annealed sheet I and II interface

shear bands density was increased with the increase in the reduction strain from 38 to 50% during the hot-rolling process. The shear band form during high strain process associated with DRX. During hot rolling, the normal strain and high temperature cause softening and local strain. Under this condition, dislocation density becomes more concentrated which is lead to form the shear bands [43–45]. SEM image of annealed sheet II shows no visible intermetallic compound; EDS point analysis provides further support as shown in Fig. 3c. In addition, EDS line scan of the annealed sheet I and II is given in Fig. 3d, which show the effect of reduction strain and heat treatment. A thin diffusion reaction layer was observed at the Ti/AZ31 interfacial zone, which resulted in atoms diffusion occurring despite the short rolling time. Since Ti-Mg binary phase diagram shows tiny mutual solid solubility, they do not react with each other; no exist of intermetallic phase [12]. Therefore, the bonding between Ti and Mg may occur by interdiffusion or intermixing at an atomic level [10, 46, 47]. The bonding strength is

a function of surface roughness and post-heat treatment. It has been reported that severe plastic deformation can produce significant mixing, such as ball milled powders and roll bonding [48, 49].

The results showed that no enrichment of Al element found across the interface of the Ti/AZ31 after annealing heat treatment, as shown in Fig. 3c. Thus, there is no possibility to form of brittle intermetallic compounds between Ti–Al and Mg–Al at the interfaces. Figure 4 showed XRD patterns of Ti, AZ31, as-rolled, and annealed clad sheet II. The AZ31 presents a strong XRD diffraction peak (0002) basal plane texture. Furthermore, there is no evidence for intermetallic compounds obtained from Ti, AZ31, as-rolled, and annealed sheet II diffraction patterns, as shown in Fig. 4c and d.

After hot rolling, (10 $\bar{1}$ 1), (10 $\bar{1}$ 0), and (11 $\bar{2}$ 0) show strong XRD diffraction peak while (0002) shows weak diffraction peak which means the material is exhibiting texture evaluation. The peak intensity should be attributed to the relative

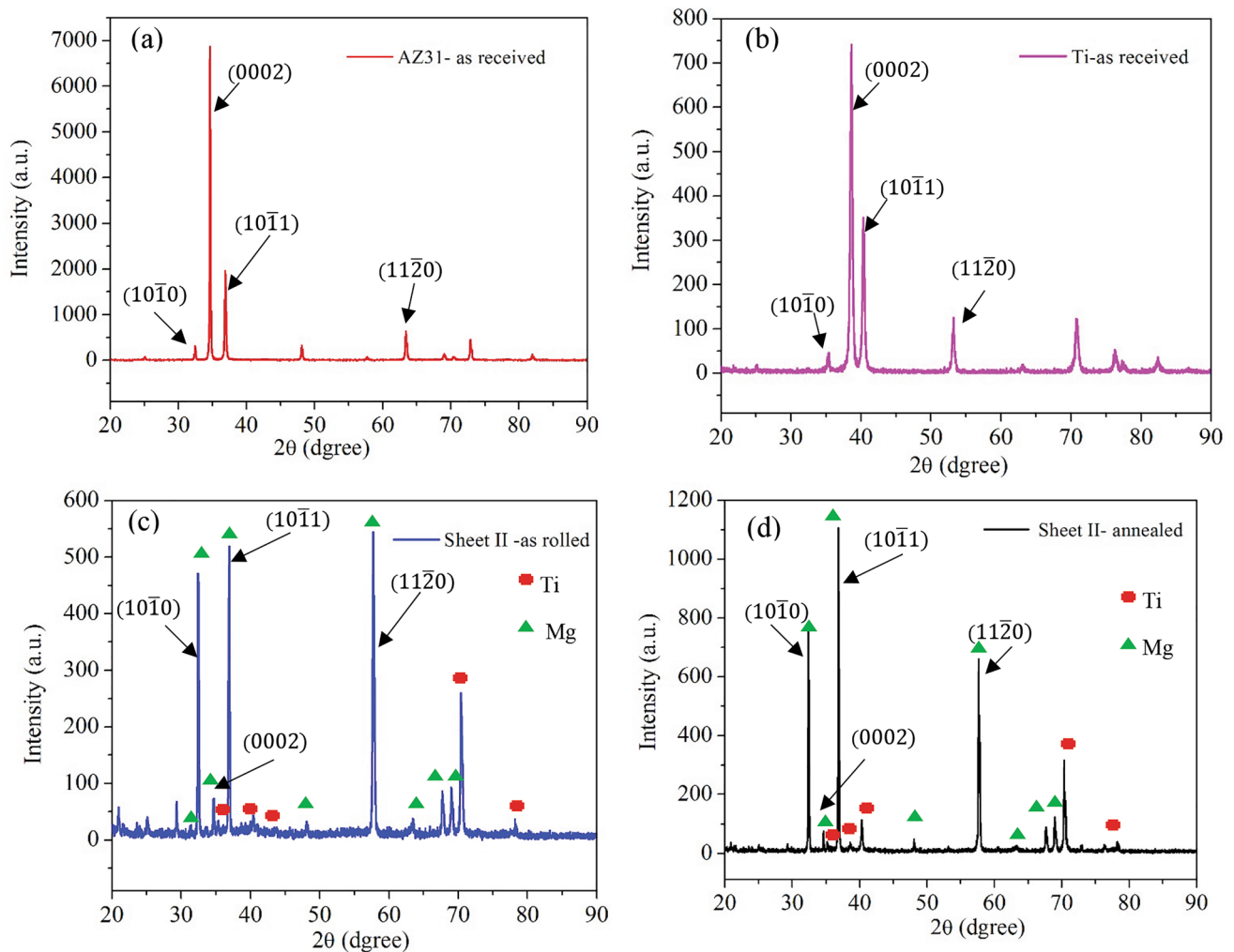


Fig. 4 Shows X-ray diffraction patterns of (a) AZ31 as-received; (b) Ti as-received; (c) sheet II as-rolled; (d) sheet II-annealed

number of crystal planes parallel to the surface [50, 51]. In addition, the reorientation of lattice was occurred by twinning that led to weak the strong basal texture. Therefore, the strong peak corresponds to the higher crystal plane. After annealing, the strong peaks remain the same, with the intensity increasing obviously.

Texture Evolution of Clad Sheets

The AZ31 Layer

The AZ31 layer is the largest substantial component of the clad sheet, and its texture significantly affects the mechanical properties. EBSD analysis investigated the texture of the AZ31 layer before and after annealing heat treatment. Figure 5 shows EBSD inverse pole figure (IPF) map, pole figures, and distributions of misorientation angle, which were obtained from areas far from the AZ31/Ti interface of the as-rolled sheet I (central part of the AZ31 layer).

Figure 5a shows IPF map and grain boundaries (GBs) which is a columnar grain structure containing deformed and fine substructure grains with an average grain size of 6.36 μm . The average grain size was calculated from IPF maps. The different color in EBSD map means different crystal orientation. The fine grains are found as resulting of the DRX during hot rolling, as discussed in the previous section. The as-rolled AZ31 layer developed strong basal crystallographic textures. The maximum pole intensity of the (0001) PF was 26.22 which tilted at 14° away from the normal direction ND toward RD, as shown in Fig. 5b. It has been reported that deformation by the basal $\langle a \rangle$ slip system ($\{0001\}\langle 11\bar{2}0 \rangle$) and twinning $\{11\bar{2}0\}$ can affect texture orientation by rotation of many grains from c-axes to the RD [24, 33, 52].

Various terms are used to describe the distribution of misorientation angles such as low angle grain boundaries (LAGBs; misorientation angle $< 15^\circ$); high angle grain boundaries (HAGBs; misorientation angle $> 15^\circ$); double

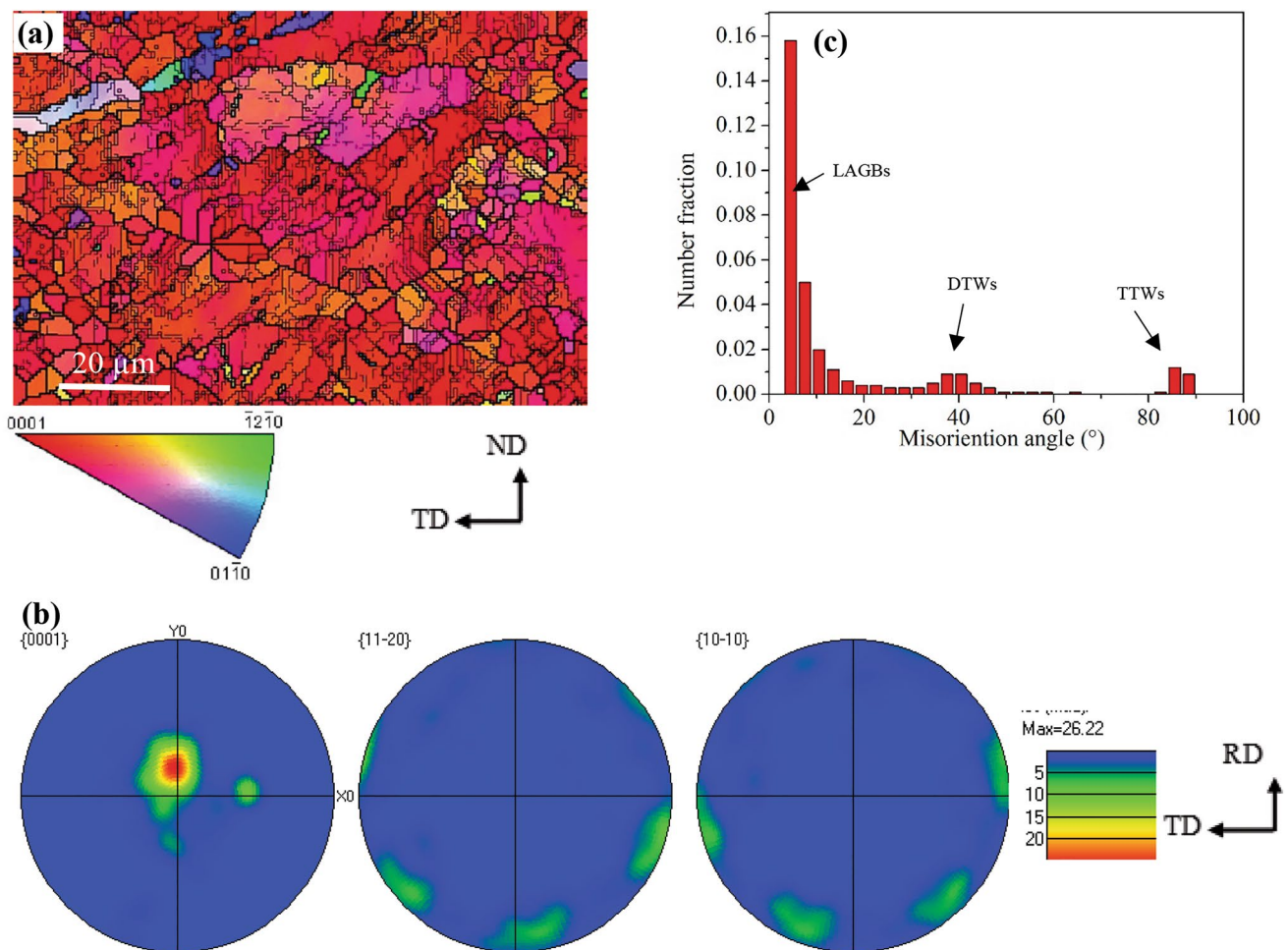


Fig. 5 Shows AZ31 layer of the as-rolled sheet I; (a) EBSD IPF image of the AZ31 layer; (b) pole figures; (c) distributions of misorientation angle

twins (DTWs; $\{10\bar{1}1\} - \{10\bar{1}2\}\langle 10\bar{2}1\rangle$) around 35° ; compression twins (CTWs; $\{10\bar{1}1\}\langle 10\bar{2}0\rangle$) around 56° ; tensile twins (TTWs; $\{10\bar{1}2\}\langle 10\bar{1}1\rangle$) around 86° [53, 54]. The distributions of misorientation angle were dominated by a large peak around 8° (LAGBs), and there are two small peaks around 40° (DTWs) and 86° (TTWs), as shown in Fig. 5c. Therefore, it is evidence that twins (TWs) and LAGBs cause the formation of shear bands during hot rolling [44, 45]. Tan et al. [55] have demonstrated that rolled AZ31 at a temperature ranging between 200 to 400 °C with high strain levels (60–80%) led to grain refinement. The IPF map contains non-indexed areas (TTWs) which subjected to high local strain (sheared during high deformation) [56]. Guan et al. [57] reported that deformed grain boundaries, deformed twins, shear bands, and second-phase particles are the main contribution to nucleation sites during the recrystallization of Mg alloys.

The sheet II was subjected to high strain (50% reduction) during the hot-rolling process. Figure 6a shows IF map

of the as-rolled AZ31 layer which also reveals a columnar grain structure (deformed and fine substructure grains) with an average grain size was $4.4\ \mu\text{m}$. The average grain size of the as-rolled AZ31 layer decreases with the increase in the reduction strain. Figure 6b shows a strong (0001) with a maximum index of 22.71 which is tilted 30° away from the normal direction ND toward RD. The texture intensity of sheet II is lower than the intensity of sheet I which is related to the amount of strain. Hot-rolled AZ31 usually exhibits (0001) pole figure orientation distribution around ND wider in RD than in TD [58]. In addition, the pyramidal slip system $\langle c + a \rangle$ ($\{1122\}\langle 11\bar{2}3\rangle$) is responsible for splitting of the basal pole toward the RD for the hot-rolled AZ31 [34, 58, 59]. Figure 6c shows distributions of misorientation angle which consist of two main peaks with rang $\sim 5^\circ\text{--}8^\circ$ and $\sim 85^\circ\text{--}90^\circ$. The first beak represents LAGBs, while the second peak represents HAGBs (TTWs; $\{10\bar{1}2\}\langle 10\bar{1}1\rangle$).

In addition to the two main peaks, there is a small fraction of double twins (DTWs; $\{10\bar{1}1\} - \{10\bar{1}2\}\langle 10\bar{2}0\rangle$)

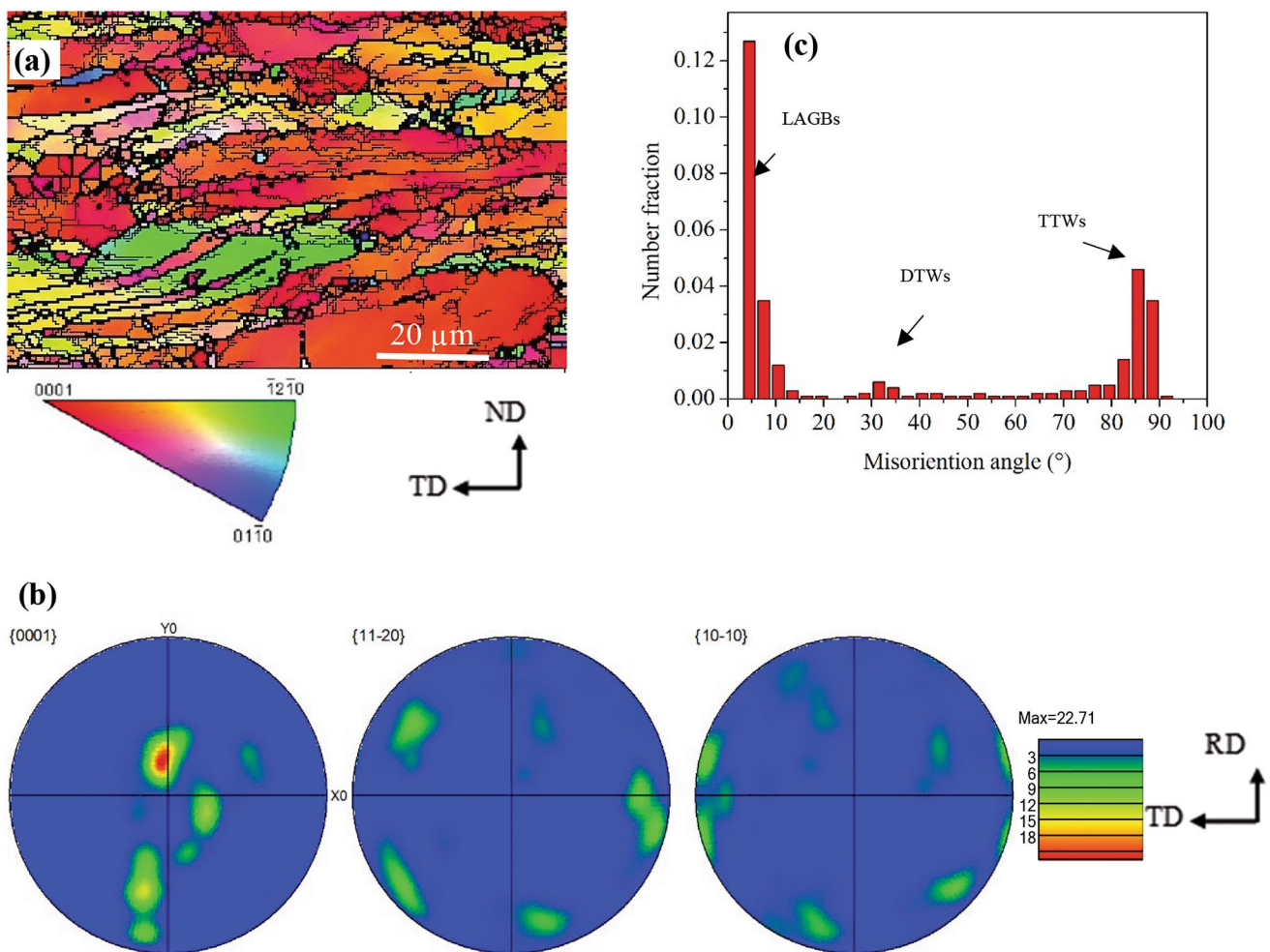


Fig. 6 Shows AZ31 layer of as-rolled sheet II; (a) EBSD IPF image of the AZ31 layer; (b) pole figures; (c) distributions of misorientation angle

around 35° [53, 54]. The number of CTWs $\{10\bar{1}1\}\langle 10\bar{2}0\rangle$ are limited because of their transformation to DTWs, $\{10\bar{1}1\} - \{10\bar{1}2\}\langle 10\bar{2}0\rangle$ [56, 60]. It has been reported that the DTWs reduce the ductility of Mg alloys and lead to shear failure at low strain [61]. Hot rolling associated with a large strain deformation leads to reduce critical resolved shear stress (CRSS) of the pyramidal $\langle c+a \rangle$ slip system and non-basal slip system may become activate [34, 62, 63]. DRX has been taken place during hot rolling for both sheet I and sheet II, which involve to convert the LAGBs to HAGBs [55].

During the annealing heat treatment, recovery, recrystallization, and grain growth have been taken place with different rates on different regions of the AZ31 layer which was depending on their local stored energies. The microstructure evaluation after annealing treatment at 400°C for 12 h shows that there is no presence of any elongated

grains which indicates that the microstructure has been recrystallized and grown to some extent.

Figure 7 shows IPF map, (0001) PF, and distributions of misorientation angle in areas far from the interface AZ31/Ti of the sheet I. Equiaxed coarse grains are formed after the heat treatment. The average grain size was $9.28\ \mu\text{m}$, as shown in Fig. 7a. The deformed grains and non-indexed areas with higher internal stored energy were recrystallized. The (0001) PF shows double-peak basal pole intensity which is tilted about $\pm 25^\circ$ from the ND toward the TD, as shown in Fig. 7b. Also, the basal texture intensity was significantly reduced from 26.22 to 7.51 [24, 34]. The annealing process has the most significant enhancement of AZ31 layer texture which was weakening the severely deformed grains of the texture component [34, 57, 64]. Qiao et al. [32] and Nie et al. [24] have reported the mechanism of LAGBs transformation into HAGBs by migration of the grain boundaries of the sub-grains. Figure 7c shows distributions of misorientation angle which is exhibited by a random distribution of grain

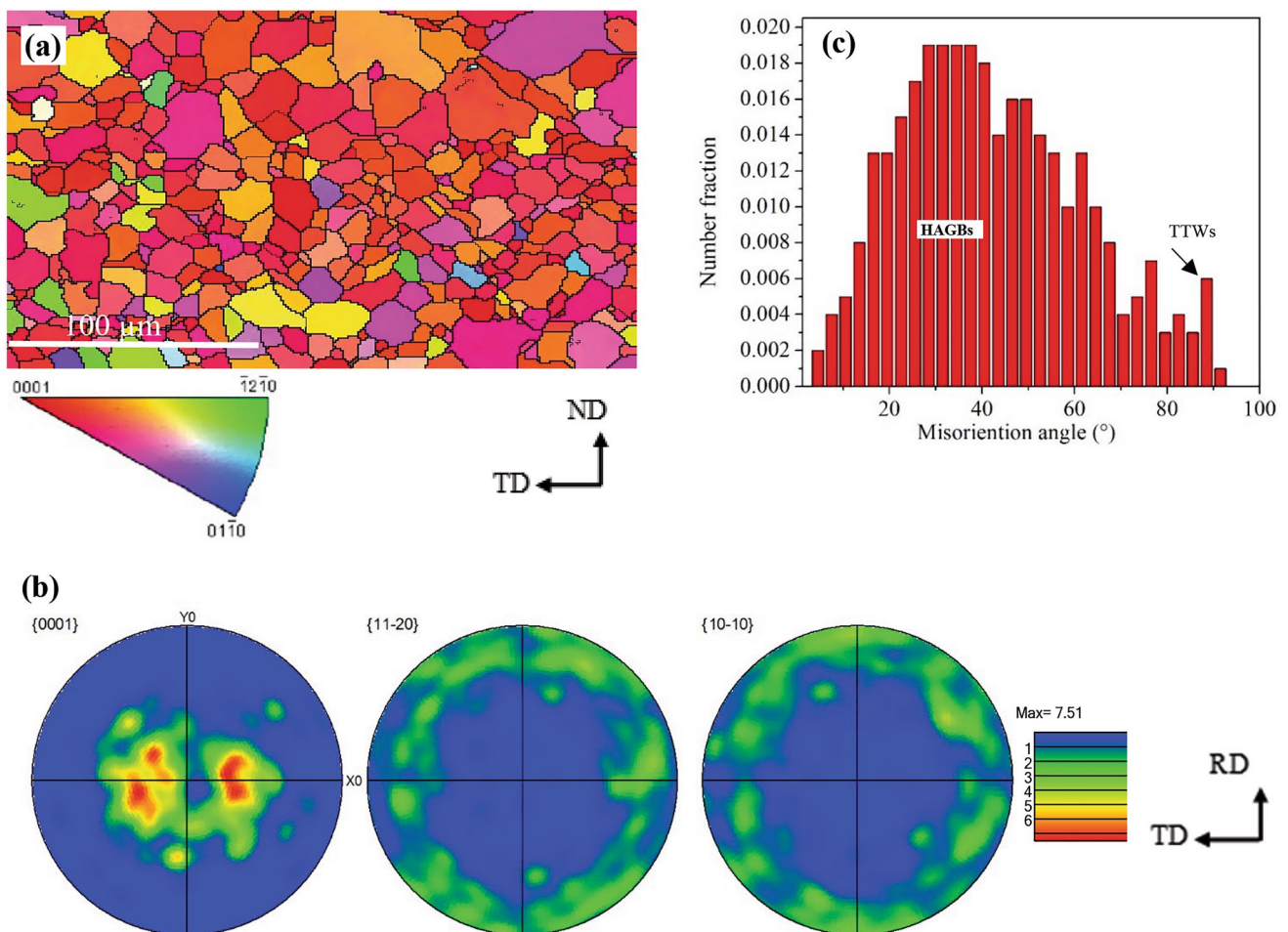


Fig. 7 Shows middle of the AZ31 layer for the annealed sheet I; (a) IPF figure of the AZ31 layer; (b) pole figures; (c) distributions of misorientation angle

boundaries with the domination of HAGBs. This indicates that the static recrystallization process (SRX) had taken place during annealing heat treatment [51, 64]. During the annealing process, the stored energy from plastic deformation could be the driving force for SRX [51, 65].

Figure 8 shows IPF map, (0001) PF, and distributions of misorientation angle in areas far from the AZ31/Ti interface after annealing of the sheet II. Figure 8a shows IPF map which reveals recrystallized texture with an average grain size of 8.97 μm . Figure 8b shows (0001) PF a significant change in pole intensity distribution compared with as-rolled sheet II. After the annealing treatment, the basal pole intensity decreased from 22.71 to 9.68. The result shows that single pole intensity maxima splitting along the RD, and a wide pole intensity distribution inclined -5° from the ND to word RD. Hong-Fei et al. [33] have been reported that the most recrystallized grains tilt away from the ND depending on the degree of deformation. Sample with deformation higher than 30% shows double pole tilts toward TD, while the sample with high plastic deformation shows tilting toward RD. The

basal plan pole tilting will affect the mechanical anisotropy along (RD) and (TD) during the tension test at room temperature. The annealing heat treatment is effective in weakening of the basal texture intensity of the as-rolled clad sheet due to SRX. Figure 8c shows a wide misorientation distribution histogram in the range of the angle between 20° and 60° (HAGBs) which confirms the SRX.

Figure 9 shows IPF map, (0001) PF, and distributions of misorientation angle in areas close to the AZ31/Ti interface after annealing of the sheet II. Coarse grains are formed at the AZ31 layer close to the interface after annealing heat treatment. The average grain size was 13.03 μm , as shown in Fig. 9a. Figure 9b shows double-peak (0001) PF with an intensity of 9.77 which is tilted about 50° from the ND toward TD. Figure 9c shows the misorientation distribution of grain boundaries which exhibit two strong beaks at $\sim 35^\circ$ and $\sim 85^\circ$. The first beak represents the recrystallized grains which support the above discussion of the increase in grain boundary misorientation and the conversion of LAGBs into HAGBs. Another peak represents the probability of existing

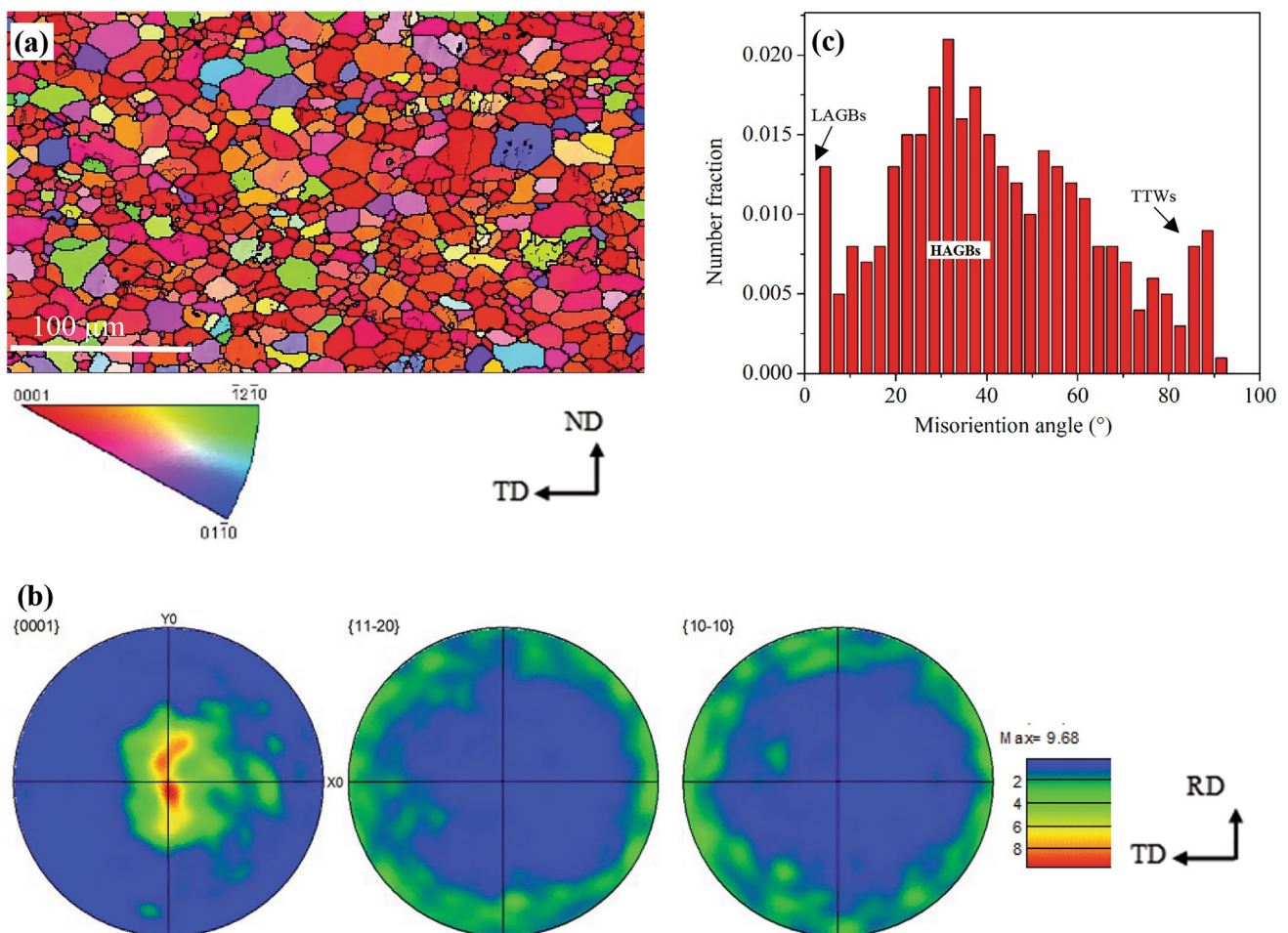


Fig. 8 Shows the middle of the AZ31 layer for annealed sheet II; (a) IPF figure of the AZ31 layer; (b) (0001) pole figure; (c) distributions of misorientation angle

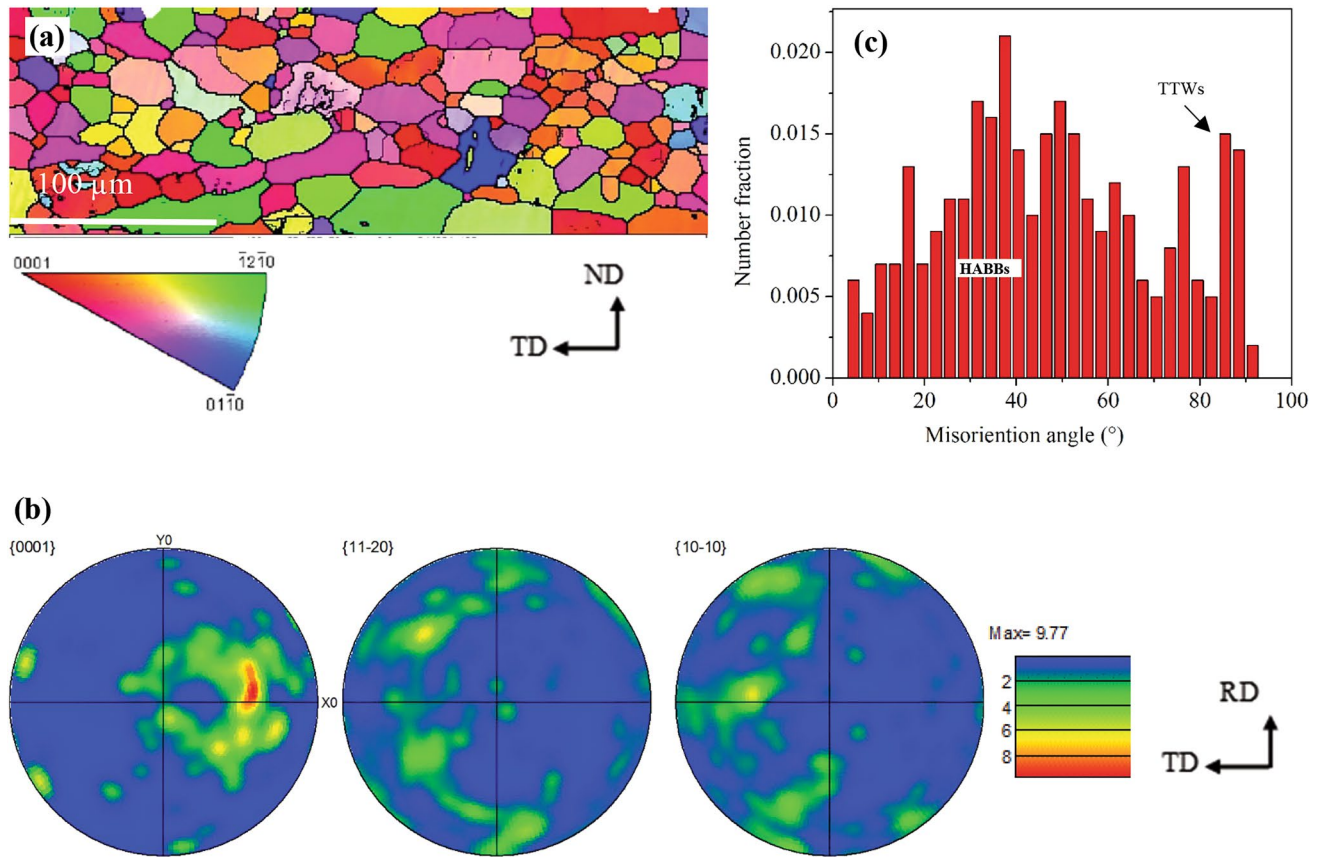


Fig. 9 Shows annealed sheet II for AZ31 layer close to interface; (a) IPF figure of the AZ31 layer; (b) (0001) pole figure; (c) distributions of misorientation angle

of the TTWs $\{10\bar{1}2\}\langle 10\bar{1}1\rangle$ [6]. The grain sizes of AZ31 layer close to the interface are larger than those in the areas far from the interface. With high friction at the interface, high deformation energy is stored which provides a larger driving force for recrystallization. It can be seen that the microstructure after annealing heat treatment become HAGBs with a small number of twins at the interface. The twins and twin-grain boundary (GB) lead to activate of nucleation which leads to form of new grains DTWs ($\{10\bar{1}1\} - \{10\bar{1}2\}\langle 10\bar{2}0\rangle$) and CTWs ($\{10\bar{1}1\}\langle 10\bar{2}0\rangle$). Chao et al. [65] suggested that high dislocation density was preferential nucleation sites during SRX of the AZ31 Mg alloy. Their observation depends on the modeling of fine grains and the twin's texture before and after annealing heat treatments. As a result of annealing heat treatment, SRX causes the weakening of AZ31 layer the basal texture which is not eliminated [57, 66]. Kawamoto et al. [12] studied Mg/Ti interface crystal orientation using EBSD. They confirm that twins formed at the interface after applying strain. Guan et al. reported that DTWs could weaken the deformed texture and for the first time provide direct evidence that

recrystallized grains originating from double twins can form the rare earth texture during annealing recrystallized grain nucleation, grain growth, and texture evolution of Mg alloy after heat treatment [56].

The Ti Layer

Figure 10 shows EBSD inverse pole figure map, (0001) PF, and distributions of the misorientation angle of the sheet I Ti layer in as-rolled and annealed state. A few studies have been reported the hot-rolling texture of pure Ti, and all investigation has been done using X-ray diffraction (XRD) pole figures [67]. The results reveal uniform grains with an average grain size of 2.83 μm and 3.35 μm for as-rolled and annealed, respectively, as shown in Fig. 10a and b. The Ti layers were subjected to low deformation strain due to different flow stress of the Ti and AZ31. In this work, a thin Ti layer (0.2 ± 0.02 mm) was used to clad the AZ31 which was subjected to shear deformation generated by friction from both the AZ31 layer and rolls. The hot-rolling and annealing heat treatment was carried out at a temperature lower than the recrystallization temperature of Ti (≥ 500 °C) [9, 10].

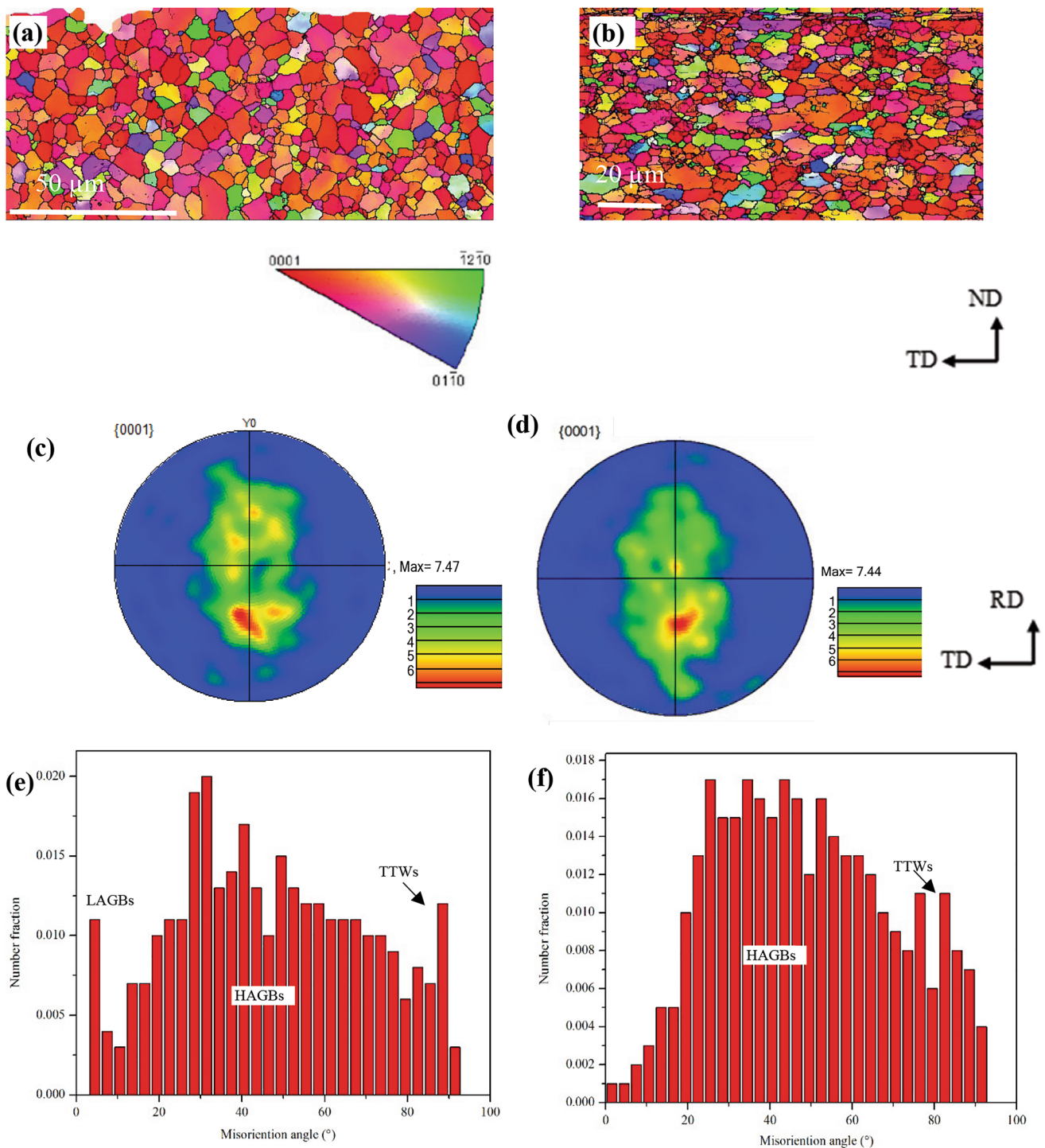


Fig. 10 Shows sheet I Ti layer in as-rolled and annealed state: **(a, b)** IPF map; **(c, d)** (0001) pole figure; **(e, f)** distributions of misorientation angle

Therefore, it is considered to be in a deformed or recovered state, i.e., unrecrystallized. The (0001) PF of as-rolled and annealed Ti layers is represented in Fig. 9c and d. There was a slight decrease in the texture intensity after annealing. Both as-rolled and annealed texture show single pole

basal texture split to the RD, and the maximum intensity of (0001) poles shifted by 35°–45° toward RD from ND. The distribution of the grain boundaries misorientation angle illustrated in Fig. 9e and f confirm a wider distribution of HAGBs in the range of the angle between 20° and 80°

with a small fraction of LAGBs and TTWs in the as-rolled layer which was disappeared after heat treatment. Dragomir et al. [68] studied hot rolled commercially pure titanium at 268 °C to a different reduction of 40–80%; they found that the (0001) PF was split to the RD in the initial state, and then, the orientation become TD at a higher strain of 80%. Bouhattate et al. [69] simulated experimental data of cold and hot-rolled commercial pure Ti texture with a different strain. They show that the (0001) PF split along RD for the hot-rolled sample with a strain of 20% for both experimental and simulated.

Figure 11 depicts EBSD inverse pole figure map, (0001) PF, and distribution of grain boundaries misorientation angles for as-rolled and annealed state sheet II. The Ti layers in the sheet II have exhibited a similar texture as in the sheet I, which is confirmed the Ti layer subjected to low deformation stain in both sheets I and II. The average grain size was 2.86 μm and 4.41 μm for as-rolled and annealed sheets, respectively, as shown in Fig. 10a and b. Also, the (0001) PF shows single pole basal texture split to the RD by 35°–45° toward RD from ND, as shown in Fig. 11c and d. The distribution of the grain

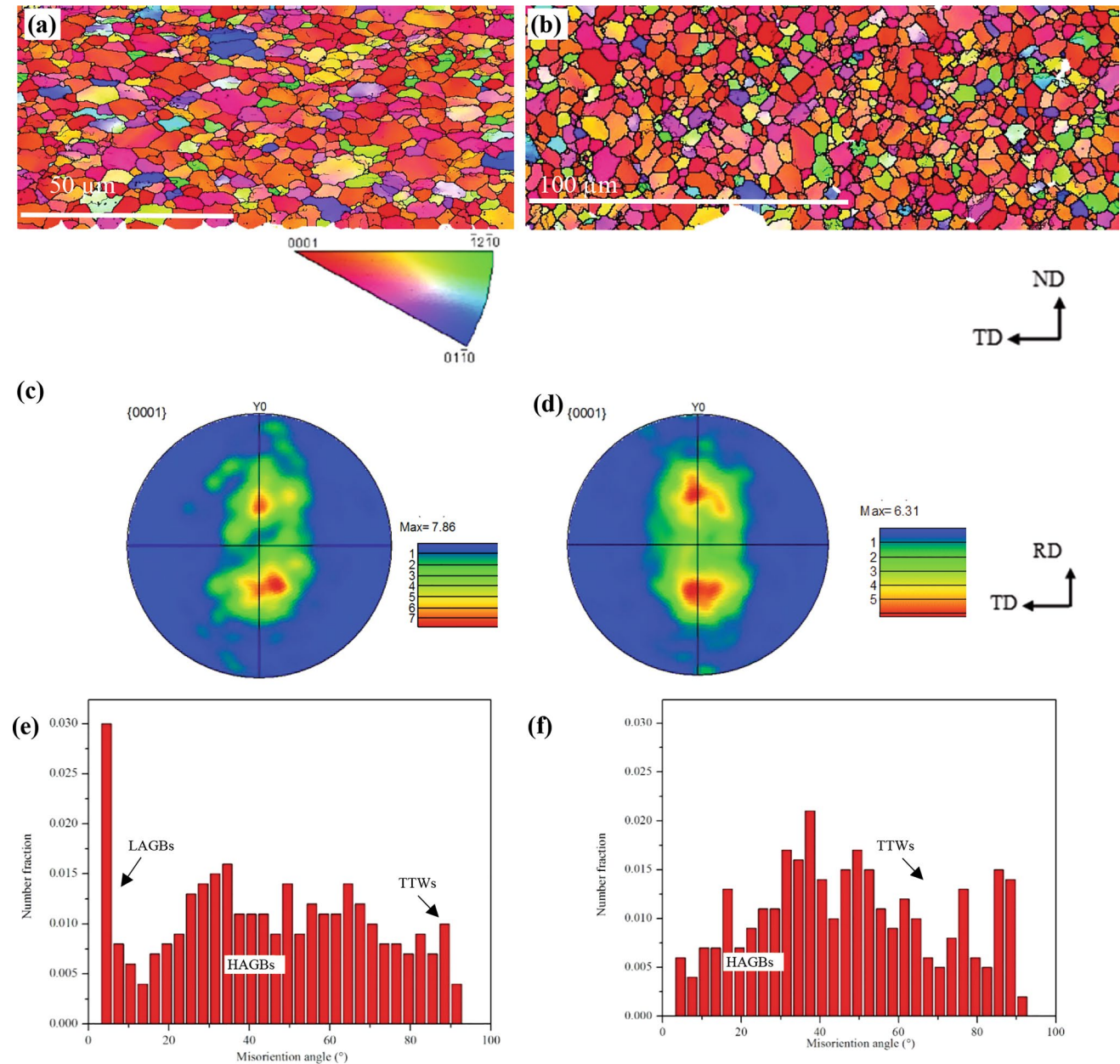


Fig. 11 Shows sheet II Ti layer in as-rolled and annealed state: (a, b) IPF map; (c, d) (0001) pole figure; (e, f) distributions of misorientation angle

boundaries misorientation angle is shown in Fig. 11e and f which exhibits HAGBs in the range of the angle between 20° and 80° with a small fraction of LAGBs and TTWs in the as-rolled sheet which was disappeared after heat treatment.

Mechanical Properties

The mechanical properties were investigated by conducting nanoindentation and tensile tests at room temperature. The annealing heat treatment process could affect the mechanical properties of the clad sheets. The effect of the clad sheets texture on the mechanical properties was studied as well.

Nanoindentation Test Results

The nanoindentation is a useful characterization technique that reflects the strength of the clad sheet layers. Nanoindentation test was conducted to study the mechanical properties of the clad sheets layers. Indentation test was performed on Ti/AZ31/Ti cross section for assembly sample, sheet I, and sheet II in as-rolled and annealed conditions, as shown in Fig. 12a. The hardness of the Ti layers is much higher than that of the AZ31 layer in all conditions. After the hot-rolling, the hardness of the AZ31 layer enhanced, while Ti layer showed a slightly increasing. The hardness of as-rolled AZ31 layer is slightly higher than the AZ31 layer in the assembly sample, which is likely associated with twins, shear bands microstructures, and high texture intensity generated during the hot-rolling process. Also, hardness

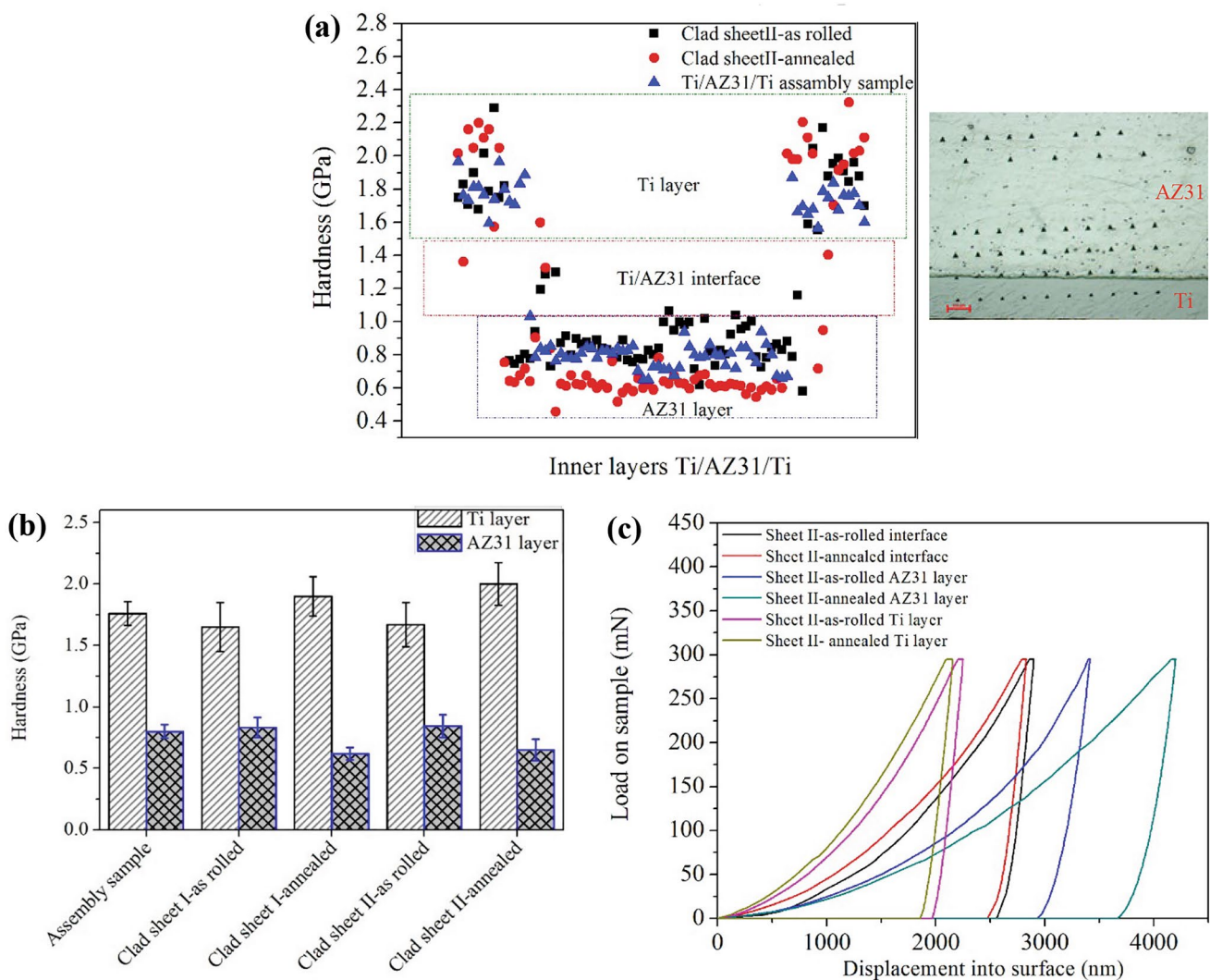


Fig. 12 (a) local nanoindentation evolution through the cross section of the sheet II; (b) average hardness values of assembly sample, the clad sheet I and II; (c) nanoindentation load–displacement curves of the sheet II

measurements showed that increase in hardness values with increasing rolling reduction. This could be attributed to fine grain size and the increase in shear band density [65, 70].

The shear bands' hardness has been discussed by Fatemi-Varzaneh et al. [44] in the AZ31 Mg alloy. Also, the shear bands may consider a grain refining mechanism. Thus, the tensile strength of the clad sheets was enhanced while reducing the ductility.

Further annealing heat treatment, the hardness of the AZ31 layer was decreased. The hardness value decreased attributed to the recovery and recrystallization during heat treatment [65, 71]. The average hardness values of the assembly sample, the clad sheet I, and sheet II are shown in Fig. 12b. The hardness of the annealed Ti layer is higher than that in assembly and as-rolled samples, which may associate with the diffusion of Al to Ti side during heat treatment [72–74]. The nanoindentation load–displacement curves of the as-rolled and annealed clad sheet II are presented in Fig. 12c. A maximum load of 30 mN was applied, and the indentation depth was in the range of 2000–3500 nm. The AZ31 layer showed quite a difference in indentation depth before and after heat treatment. The hardness values are increasing, and the indentation depth decreasing agrees with the fact that hardness has increased with the higher resistance of the as-AZ31 layer to the indenter.

The Tensile Properties of Clad Sheets

Figure 13a shows the stress–strain curves of the AZ31 and clad sheet II (as-rolled and annealed conditions). The tensile properties are summarized in Fig. 13b; for the ultimate tensile strength (UTS), 0.2% yield stress (YS), and the elongation in the RD and TD directions. The tensile tests were

conducted at room temperature. The as-rolled sheets show that increased the flow stress and significantly decreased the elongation. The UTS and YS of as-rolled sheet II reached 365 MPa and 280 MPa, respectively, which was ~26% and 25% higher than that of AZ31 alloy (290 MPa and 224 MPa). The elongation was 13% which was ~23% lower than that of AZ31 alloy (17%). This is generally attributed to dislocation strengthening mechanisms during the hot-rolling process in which the higher density of dislocations and finer microstructures (twins and shear bands) pinned the dislocations and caused strengthening in the AZ31 layer. In general, materials processed through severe plastic deformation showing very limited ductility due to the fine-grained microstructure. It is reported that shear bands act as stress concentration point which leads to the failure of the materials at low elongation [40, 41].

It can be seen that the annealed sheets exhibit lower UTS and YS than the as-rolled sheets which are a good agreement with the texture evolved after the heat treatment. The clad sheets mechanical properties are controlled by the component's texture and layered structural design. The elongation of the sheet II is significantly improved following the annealing treatment at 400 °C for 12 h. The elongation reached 35% and 26% in RD and TD, respectively, which is ~51% and 35% higher than of as-received AZ31. The AZ31 is the largest constituent layer in the clad sheets which controls the mechanical performance due to its sensitivity to cracks [26]. Therefore, the annealing heat treatment is highly significant. The texture evolution of the AZ31 layer obtained by annealing heat treatment is the essential step to improve the sheets mechanical properties. On the other hand, the Ti cladding layer has better formability than the AZ31 alloy which may impose

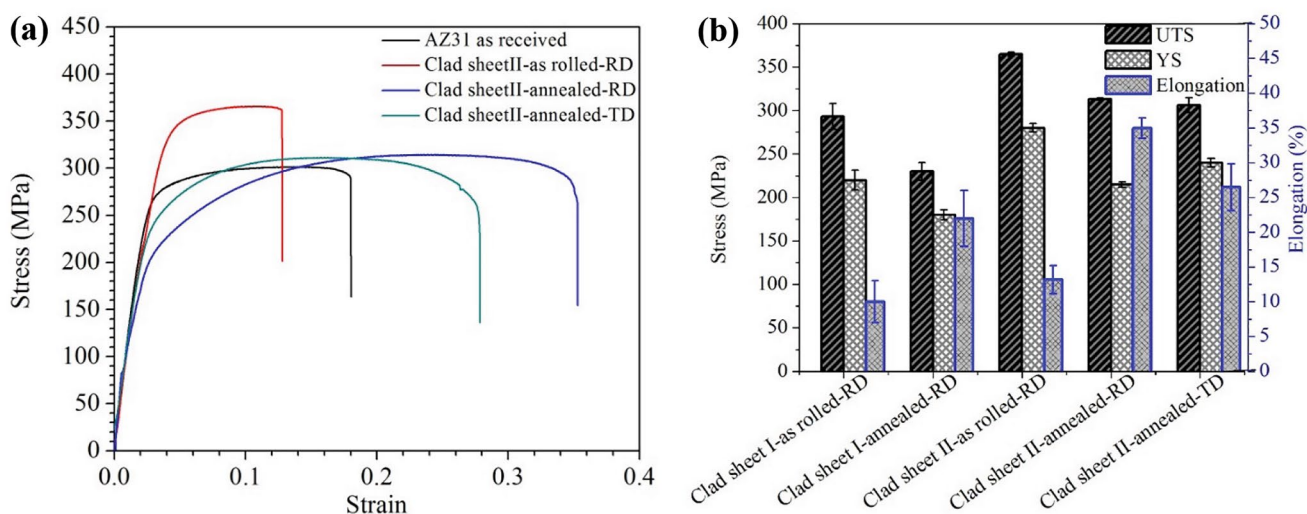


Fig. 13 (a) stress–strain curves of the AZ31 and clad sheet II in as-rolled and annealed conditions; (b) summarized average of the UTS, YS, and the elongation

the maximum tensile stress. However, the Ti layers were subjected to work hardening due to mechanical cleaning and rolling processes [9]. Therefore, Ti may fail at lower elongation since the annealing heat treatment is carried out at a temperature lower than Ti recrystallization temperature. The mechanical performance of the clad sheet can be calculated using the rule of mixtures (Eq 1) [26, 75]

$$\sigma_{clad} = \sigma_{Ti} * v_{Ti} + \sigma_{AZ31} * v_{AZ31} \quad (1)$$

where σ_{clad} is the strength of the clad sheet; (σ_{Ti} ; σ_{AZ31}) and (v_{Ti} ; v_{AZ31}) are the strength and volume fractions of Ti and AZ31, respectively. The results show that the experimental result agrees with the theoretical calculation (the calculated results provided in the supplementary materials). The bonding strength between the AZ31/Ti plays a critical role in the mechanical properties of the clad sheets. It has been reported that interface bonding affects load transfer and the stress redistribution during the deformation [26, 75]. Kawamoto et al. [28] studied stain transfer through Mg/Ti interface. They found that the Mg twinning is associated with Ti dislocation motion. In this study, the AZ31/Ti interface crystallographic orientation is controlled by AZ31 twinning, which agrees with Kawamoto et al. conclusion; AZ31/Ti crystallographic orientation is provided in the supplementary materials. Brittle/ductile composite materials can sustain large plastic deformation without failure through the structure design such as layered, networks, and bi-layer. Huang et al. [75] studied the strain delocalization and constrained crack distribution of layered Ti/Al composite material. They found that constrain interface may restrict the extensive crack and relieve the localized strain at the interface. The elongation of the sheet II in the RD and TD directions shows 35% and 26%, respectively, which is related to the anisotropic properties of AZ31 layer texture. It can be seen that the YS of the sheet depends on the sample direction; where the TD tensile samples show an increase in the YS and a decrease in elongation compared to the RD samples [9]. In addition, the mechanical properties of the sheet II are same as or higher than that of magnesium alloy that is processed by plastic deformation and annealed [51, 62, 70]. Therefore, the sheet II exhibits a combination of strength and ductility and suggested that the shape of (0001) basal plane effect the planer anisotropy, which means the probability of activation slip systems according to the Schmid factor in RD is higher than TD [9, 58, 59].

The sheet II presented ductility behavior higher than the AZ31, which is related to the unique layered structural design. As shown in Fig. 13b, the annealed sheets II showed better mechanical properties than those of sheet I. The reasons for these variations can be related to the bonding strength between the Ti/AZ31, which enhanced as a function of large rolling reduction and post-heat treatment.

This is further support for the effect of the interdiffusion layer on the interface strength.

Fracture Morphology of Clad Sheets

The fracture surface of the sheet II in as-rolled and annealed conditions is shown in Fig. 14. The fracture was governed by the failure of the AZ31 layer, nucleation, and growth of cracks. Compared to the failure surface of the sheet II before and after annealing treatment, the Ti layers in both conditions show equiaxed dimples on the failure surface, which leads to ductile fracture of the Ti layer, as shown in Fig. 13a and b. Figure 9c shows the surface of the as-rolled AZ31 layer with large voids (indicated by a red circle), shear bands (indicated by a blue arrow), and tear ridges (indicated by a yellow arrow). The fracture surface features are typical intergranular fracture that occurs due to high dislocation densities (shear bands). As a result, shear bands areas are potential stress concentration sites which susceptible to void and crack formation starting early. This causes a reduction in the clad sheet ductility [40]. After annealing, the AZ31 layer exhibits ductile fractures with fine equiaxed dimples that lead to a significant increase in tensile ductility, as shown in Fig. 14d. Thus, modifying the shear banding structure can lead to relatively high elongation. Subsequent annealing heat treatment is believed to recover and recrystallize the deformed materials, which leads to homogenous microstructure and delays the cracking formation in AZ31 layer.

Conclusions

The single-pass hot-rolling and annealing heat treatment would be a successful way to fabricate lightweight Ti/AZ31/Ti clad sheets with excellent corrosion resistance and mechanical properties. The tensile test was performed at RT for as-rolled and annealed clad sheets which reflect the heat treatment on the changes of the microstructure and texture. The AZ31 layer controlled the tensile properties of the clad sheets since it is the major component of the clad sheet. The clad sheets showed strong basal texture in the AZ31 layer due to twins and shear bands. The shear bands were caused by the strain localization which leads to the failure of the sheets at lower elongation. The texture of the AZ31 layer was significantly improved after the annealing heat treatment (i.e., SRX) at 400 °C for 12 h. The clad sheets elongation was improved by flowing annealing heat treatment which was explained by the texture evolution in the AZ31 layer and interfacial bonding strength between the Ti–AZ31. The sheet II showed the best mechanical properties with the YS, UTS, and elongation reaching 215 MPa, 313 MPa and 35%, respectively, in the RD and 240 MPa, 306 MPa and 26%, respectively, in the 26.46 TD.

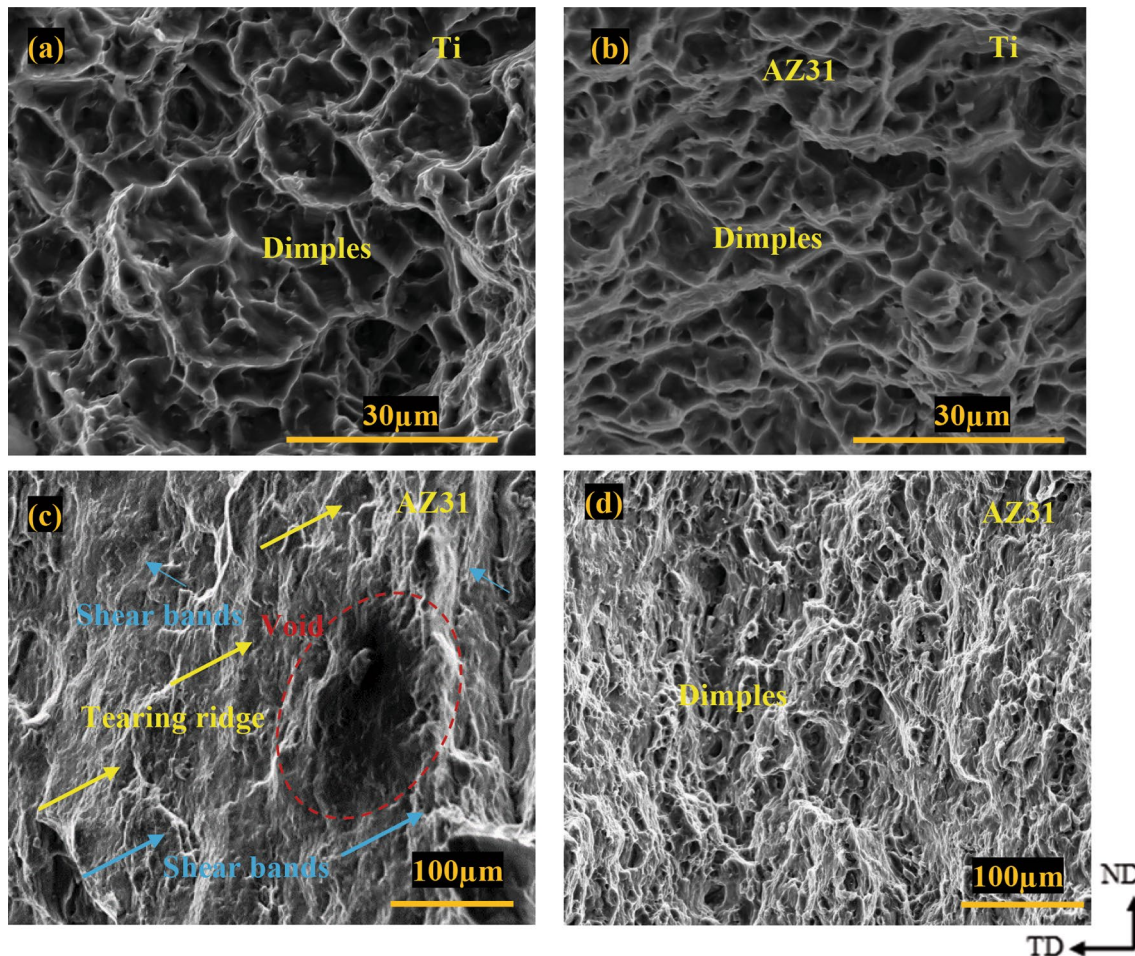


Fig. 14 SEM of tensile fracture profile of the Sheet II (a) as-rolled and (b) annealed Ti layer; (c) as-rolled and (d) annealed-AZ31 layer

Acknowledgements This study was partially supported by the Higher Committee for Education Development (HCED) in Iraq and the University of Kentucky. The author gratefully acknowledges helpful discussions with Prof. Yang-Tse Cheng and Fuqian Yang/University of Kentucky chemical and materials engineering department with thanks.

Conflict of interests The author declare that have no known competing financial interests or personal relationships that could have appeared to influence the work reported in this paper.

References

1. H. Chang et al., Texture evolution of the Mg/Al laminated composite fabricated by the accumulative roll bonding. *Scripta Mater.* **61**(7), 717–720 (2009)
2. R.N. Dehsorkhi, F. Qods, M. Tajally, Investigation on microstructure and mechanical properties of Al–Zn composite during accumulative roll bonding (ARB) process. *Mater. Sci. Eng. A.* **530**, 63–72 (2011)
3. M.M. Mahdavian, L. Ghalandari, M. Reihanian, Accumulative roll bonding of multilayered Cu/Zn/Al: an evaluation of microstructure and mechanical properties. *Mater. Sci. Eng. A.* **579**, 99–107 (2013)
4. A. Mozaffari, H. Danesh Manesh, K. Janghorban, Evaluation of mechanical properties and structure of multilayered Al/Ni composites produced by accumulative roll bonding (ARB) process. *J. Alloys Compd.* **489**(1), 103–109 (2010)
5. L.Y. Sheng, F. Yang, T.F. Xi, C. Lai, H.Q. Ye, Influence of heat treatment on interface of Cu/Al bimetal composite fabricated by cold rolling. *Compos. Part B Eng.* **42**(6), 1468–1473 (2011)
6. H. Nie et al., The microstructure, texture and mechanical properties of the rolled Al/Mg/Al clad sheets. *J. Mater. Eng. Perform.* **25**(11), 4695–4705 (2016)
7. J.-S. Kim et al., Improvement of interfacial bonding strength in roll-bonded Mg/Al clad sheets through annealing and secondary rolling process. *Mater. Sci. Eng. A.* **628**, 1–10 (2015)
8. A. Çetin et al., Laminated metal composites by infiltration. *Metall. Mater. Trans. A.* **42**(11), 3509–3520 (2011)
9. H. Inoue, M. Ishio, T. Takasugi, Texture, tensile properties and press formability of Mg–3Al–1Zn/Ti clad sheets produced by roll-bonding. *Mater. Sci. Forum.* **495–497**, 645–650 (2005)

10. Inoue, H., Mechanical Properties and Formability of Titanium-Clad Magnesium Alloy Sheets. In: *Proceedings of the 8th Pacific Rim International Congress on Advanced Materials and Processing* (Springer, Cham, 2013), p. 1109–1114.
11. B. Alobaid, F. Yang, Y.-T. Cheng, Microstructure and deformation behavior of hot-rolled AZ31/Ti multilayers. *Mater. Res. Express.* **6**(8), 0865a2 (2019)
12. H. Kawamoto et al., Analysis of strain transfer through the Mg/Ti interface using crystallographic orientation analysis based on electron back-scattered diffraction patterns. *Mater. Trans.* **49**(5), 1107–1111 (2008)
13. B. Alobaid, Microstructure and mechanical properties of Ti particles reinforced AZ31–Mg alloy matrix composites through ARB and subsequent annealing. *Metallogr. Microstruct. Anal.* **11**, 761–773 (2022)
14. H.S. Liu, B. Zhang, G.P. Zhang, Microstructures and mechanical properties of Al/Mg alloy multilayered composites produced by accumulative roll bonding. *J. Mater. Sci. Technol.* **27**(1), 15–21 (2011)
15. A.A.K. Ozgur Duygulu, G. Oktay, F.C. Sahin, Diffusion bonding of magnesium, zirconium and titanium as implant material. *Mater. Sci. Forum.* **546**(549), 417–420 (2007)
16. Y. Wei et al., Formation process of the bonding joint in Ti/Al diffusion bonding. *Mater. Sci. Eng. A.* **480**(1–2), 456–463 (2008)
17. C. Liu et al., Polishing-assisted galvanic corrosion in the dissimilar friction stir welded joint of AZ31 magnesium alloy to 2024 aluminum alloy. *Mater. Charact.* **60**(5), 370–376 (2009)
18. M. Aonuma, K. Nakata, Effect of alloying elements on interface microstructure of Mg–Al–Zn magnesium alloys and titanium joint by friction stir welding. *Mater. Sci. Eng. B.* **161**(1–3), 46–49 (2009)
19. L. Commin et al., Friction stir welding of AZ31 magnesium alloy rolled sheets: influence of processing parameters. *Acta Mater.* **57**(2), 326–334 (2009)
20. L. Liu, D. Ren, F. Liu, A review of dissimilar welding techniques for magnesium alloys to aluminum alloys. *Materials.* **7**(5), 3735–3757 (2014)
21. C. Tan et al., Microstructure and mechanical properties of laser welded-brazed Mg/Ti joints with AZ91 Mg based filler. *Mater. Des.* **99**, 127–134 (2016)
22. I. Topic, H.W. Höppel, M. Göken, Friction stir welding of accumulative roll-bonded commercial-purity aluminium AA1050 and aluminium alloy AA6016. *Mater. Sci. Eng. A.* **503**(1–2), 163–166 (2009)
23. C. Xu et al., Tungsten inert gas welding-brazing of AZ31B magnesium alloy to TC4 titanium alloy. *J. Mater. Sci. Technol.* **32**(2), 167–171 (2016)
24. H. Nie et al., Texture evolution of single-pass hot-rolled 5052/AZ31/5052 clad sheets. *Jom.* **68**(8), 2274–2287 (2016)
25. A. Yahiro, T. Masui, T. Yoshida, Development of nonferrous clad plate and sheet by warm rolling with different temperature of materials. *ISIJ Int.* **31**(6), 647–654 (1991)
26. B. Feng et al., On the rule of mixtures for bimetal composites. *Mater. Sci. Eng. A.* **704**, 173–180 (2017)
27. L. Li, K. Nagai, F. Yin, Progress in cold roll bonding of metals. *Sci. Technol. Adv. Mater.* **9**(2), 023001 (2008)
28. H. Kawamoto, S. Miura, K. Yano, K. Ohkubo, T. Mohri, Analysis of strain transfer through the Mg/Ti interface using crystallographic orientation analysis based on electron back-scattered diffraction patterns. *Mater. Trans.* **49**(5), 1107–1111 (2008)
29. G.F. Vander Voort, S. R. Lampman, B. R. Sanders, G. J. Anton, C. Polakowski, J. Kinson, K. Muldoon, S. D. Henry, and W. W. Scott Jr. ASM handbook. In: *Metallography and Microstructures* (Vol. 9, ASM Handbook, 2004), p. 44073–0002.
30. N. Kashaev et al., Comparative study of mechanical properties using standard and micro-specimens of base materials Inconel 625, Inconel 718 and Ti-6Al-4V. *J. Market. Res.* **2**(1), 43–47 (2013)
31. J.S. Kim et al., Novel strip-cast Mg/Al clad sheets with excellent tensile and interfacial bonding properties. *Sci. Rep.* **6**, 26333 (2016)
32. Y. Qiao et al., Microstructures, textures and mechanical properties evolution during cold drawing of pure Mg. *Microsc. Res.* **01**(02), 8–15 (2013)
33. H.-F. Sun, S.-J. Liang, E.-D. Wang, Mechanical properties and texture evolution during hot rolling of AZ31 magnesium alloy. *Trans. Nonferrous Met. Soc. China.* **19**, 349–354 (2009)
34. H.F. Sun, S.J. Liang, E.D. Wang, Mechanical properties and texture evolution during hot rolling of AZ31 magnesium alloy. *Trans. Nonferrous Met. Soc. China.* **19**, 349–354 (2009)
35. L. Guo, F. Fujita, Influence of rolling parameters on dynamically recrystallized microstructures in AZ31 magnesium alloy sheets. *J. Magnes. Alloys.* **3**(2), 95–105 (2015)
36. K. Hamad, Y.G. Ko, A cross-shear deformation for optimizing the strength and ductility of AZ31 magnesium alloys. *Sci. Rep.* **6**, 29954 (2016)
37. J.C. Tan, M.J. Tan, Dynamic continuous recrystallization characteristics in two stage deformation of Mg–3Al–1Zn alloy sheet. *Mater. Sci. Eng. A.* **339**, 124–132 (2003)
38. W.P. Jia et al., Texture evolution of AZ31 magnesium alloy sheets during warm rolling. *J. Alloys Compd.* **645**, 70–77 (2015)
39. Y. Wang et al., Formation and microstructure of shear bands during hot rolling of a Mg–6Zn–0.5Zr alloy plate with a basal texture. *J. Alloys Compd.* **644**, 147–154 (2015)
40. S. Sandlöbes et al., The relation between ductility and stacking fault energies in Mg and Mg–Y alloys. *Acta Mater.* **60**(6–7), 3011–3021 (2012)
41. Z.-Z. Shi, X.-F. Liu, Characteristics of cross grain boundary contraction twin pairs and bands in a deformed Mg alloy. *J. Alloys Compd.* **692**, 274–279 (2017)
42. Y.B. Chun, C.H.J. Davies, Texture effects on development of shear bands in rolled AZ31 alloy. *Mater. Sci. Eng. A.* **556**, 253–259 (2012)
43. S.E. Ion, F.J. Humphreys, S.H. White, Dynamic recrystallisation and the development of microstructure during the high temperature deformation of magnesium. *Acta Metall.* **30**(10), 1909–1919 (1982)
44. S.M. Fatemi-Varzaneh, A. Zarei-Hanzaki, J.M. Cabrera, Shear banding phenomenon during severe plastic deformation of an AZ31 magnesium alloy. *J. Alloys Compd.* **509**(9), 3806–3810 (2011)
45. H. Yan et al., Twins, shear bands and recrystallization of a Mg–2.0%Zn–0.8%Gd alloy during rolling. *Scripta Mater.* **64**(2), 141–144 (2011)
46. J.H. Dai et al., First principles study on stability and hydrogen adsorption properties of Mg/Ti interface. *Phys. Chem. Chem. Phys.* **17**(25), 16594–16600 (2015)
47. A. Baldi et al., Mg/Ti multilayers: Structural and hydrogen absorption properties. *Phys. Rev. B.* **81**(22), 224203 (2010)
48. K. Asano, H. Enoki, E. Akiba, Synthesis process of Mg–Ti BCC alloys by means of ball milling. *J. Alloys Compd.* **486**(1–2), 115–123 (2009)
49. S. Rousselot, D. Guay, L. Roué, Synthesis of fcc Mg–Ti–H alloys by high energy ball milling: Structure and electrochemical hydrogen storage properties. *J. Power Sources.* **195**(13), 4370–4374 (2010)
50. X. Lei et al., Microstructure and mechanical properties of magnesium alloy AZ31 processed by compound channel extrusion. *Mater. Trans.* **52**(6), 1082–1087 (2011)

51. A. Jäger et al., Influence of annealing on the microstructure of commercial Mg alloy AZ31 after mechanical forming. *Mater. Sci. Eng. A.* **432**(1–2), 20–25 (2006)
52. S. Choi, E. Shin, B. Seong, Simulation of deformation twins and deformation texture in an AZ31 Mg alloy under uniaxial compression. *Acta Mater.* **55**(12), 4181–4192 (2007)
53. H.J. Yang et al., EBSD study on deformation twinning in AZ31 magnesium alloy during quasi-in-situ compression. *Adv. Eng. Mater.* **10**(10), 955–960 (2008)
54. K.K. Alaneme, E.A. Okotete, Enhancing plastic deformability of Mg and its alloys—A review of traditional and nascent developments. *J. Magnes. Alloys.* **5**(4), 460–475 (2017)
55. J.C. Tan, M.J. Tan, Dynamic continuous recrystallization characteristics in two stage deformation of Mg–3Al–1Zn alloy sheet. *Mater. Sci. Eng. A.* **339**(1), 124–132 (2003)
56. D. Guan, W.M. Rainforth, J. Gao, J. Sharp, B. Wynne, L. Ma, Individual effect of recrystallisation nucleation sites on texture weakening in a magnesium alloy: Part 1- double twins. *Acta Mater.* **135**, 14–24 (2017)
57. D. Guan, W.M. Rainforth, L. Ma, B. Wynne, J. Gao, Twin recrystallization mechanisms and exceptional contribution to texture evolution during annealing in a magnesium alloy. *Acta Mater.* **126**, 132–144 (2017)
58. H. Yan, R.S. Chen, E.H. Han, Room-temperature ductility and anisotropy of two rolled Mg–Zn–Gd alloys. *Mater. Sci. Eng. A.* **527**(15), 3317–3322 (2010)
59. F. Kaiser, J. Bohlen, D. Letzig, K.U. Kainer, A. Styczynski, C. Hartig, Influence of rolling conditions on the microstructure and mechanical properties of magnesium sheet AZ31. *Adv. Eng. Mater.* **5**(12), 891–896 (2003)
60. S. Niknejad, S. Esmaeili, N.Y. Zhou, The role of double twinning on transgranular fracture in magnesium AZ61 in a localized stress field. *Acta Mater.* **102**, 1–16 (2016)
61. M.R. Barnett, Twinning and the ductility of magnesium alloys. *Mater. Sci. Eng. A.* **464**(1–2), 8–16 (2007)
62. D. Luo et al., Effect of rolling route on microstructure and tensile properties of twin-roll casting AZ31 Mg alloy sheets. *Materials (Basel).* **9**(6), 433 (2016)
63. Y. Qin et al., Microstructure and texture evolution in multi-pass warm rolled AZ31 magnesium alloy. *MATEC Web Conf.* **21**, 03003 (2015)
64. Q. Miao et al., Fabrication of excellent mechanical properties AZ31 magnesium alloy sheets by conventional rolling and subsequent annealing. *Mater. Sci. Eng. A.* **528**(22–23), 6694–6701 (2011)
65. H.Y. Chao et al., Static recrystallization kinetics of a heavily cold drawn AZ31 magnesium alloy under annealing treatment. *Mater. Charact.* **62**(3), 312–320 (2011)
66. J.Y. Li et al., Effects of annealing treatment on texture and stamping properties of AZ31 magnesium alloy. *Mater. Sci. Forum.* **686**, 101–106 (2011)
67. A.K. Singh, R.A. Schwarzer, Texture and anisotropy of mechanical properties in titanium and its alloys. *Z. Metallkd.* **91**(9), 702 (2000)
68. I.C. Dragomir et al., Evolution of dislocation density and character in hot rolled titanium determined by X-ray diffraction. *Mater. Charact.* **55**(1), 66–74 (2005)
69. J. Bouhattate et al., Texture prediction of cold- and hot-rolled titanium using processing path model. *J. Mater. Eng. Perform.* **20**(2), 177–184 (2010)
70. Y.G. Ko, K. Hamad, Structural features and mechanical properties of AZ31 Mg alloy warm-deformed by differential speed rolling. *J. Alloys Compd.* **744**, 96–103 (2018)
71. L. Lu et al., Effect of annealing on microstructure evolution and mechanical property of cold forged magnesium pipes. *Mater. Des.* **39**, 131–139 (2012)
72. J.-G. Luo, V.L. Acoff, Using cold roll bonding and annealing to process Ti/Al multi-layered composites from elemental foils. *Mater. Sci. Eng. A.* **379**(1–2), 164–172 (2004)
73. D. Yang et al., Ultrafine equiaxed-grain Ti/Al composite produced by accumulative roll bonding. *Scripta Mater.* **62**(5), 321–324 (2010)
74. V. Maier, H.W. Höppel, M. Göken, Nanomechanical behaviour of Al-Ti layered composites produced by accumulative roll bonding. *J. Phys: Conf. Ser.* **240**, 012108 (2010)
75. M. Huang et al., Revealing extraordinary tensile plasticity in layered Ti-Al metal composite. *Sci. Rep.* **6**, 38461 (2016)

Publisher's Note Springer Nature remains neutral with regard to jurisdictional claims in published maps and institutional affiliations.

Springer Nature or its licensor (e.g. a society or other partner) holds exclusive rights to this article under a publishing agreement with the author(s) or other rightsholder(s); author self-archiving of the accepted manuscript version of this article is solely governed by the terms of such publishing agreement and applicable law.